Influence of operating conditions on the optical optimization of solar selective absorber coatings

Antoine Grosjean, Audrey Soum-Glaude, Thomas Laurent

Version of Record: https://www.sciencedirect.com/science/article/pii/S0927024821003238
Manuscript_e32b256bb5bcb0c3a95c8e2460dc1a60

Influence of operating conditions on the optical optimization of solar selective absorber coatings

Antoine Grosjean[1,2], Audrey Soum-Glaude[3,*], Laurent Thomas[1,2]

[1] PROMES-CNRS, UPR 8521, Rambla de la thermodynamique, Tecnosud, 66100 Perpignan, France.
[2] Université de Perpignan, 52 avenue Paul Alduy, 66820 Perpignan, France.
[3] PROMES-CNRS, UPR 8521, 7 rue du Four Solaire, 66120 Font-Romeu-Odeillo-Via, France.
*corresponding author: audrey.soum-glaude@promes.cnrs.fr

Abstract: In concentrated solar power (CSP), selective solar absorber coatings increase absorbed solar flux (high solar absorptance A_S) while reducing radiative losses (low thermal emittance E_{BB}). Coating developers usually maximize the selective ratio A_s/E_{BB} (highest A_s, lowest E_{BB}). The solar-to-heat conversion (heliothermal) efficiency R_h of a solar absorber is however a more relevant optimization target. It is deduced from A_s and E_{BB}, but is more sensitive to A_s. It also strongly depends on operating conditions, solar concentration ratio C and absorber temperature T_A, radically varying between CSP technologies. This allows different optimal designs and leads to more efficient selective coatings, adapted to their specific application. In this paper, the influence of operating conditions on the optimal selective coating design is investigated. A popular selective coating design, W/W-Al_2O_3/Al_2O_3, was chosen as illustrative example. Coating structure and composition, i.e., cermet composition and layer thicknesses, were optimized to maximize R_h for a wide range of operating conditions: concentration ratios from 10 to 300, absorber temperatures from 50 to 550°C. Optimal coating characteristics are illustrated on 3D maps over the entire (C, T_A) range, showing the existence of three operating regions. Each region gives an optimization priority on either A_s, E_{BB} or a combination of both, leading to specific optimized coating characteristics for each region, which should be considered when designing selective coatings for given operating conditions. Based on one example, this study provides a better understanding of the optimal design and use of selective coatings in the different operating conditions of CSP technologies.

Keywords: Concentrated solar power, solar selective absorber coatings, optical optimization

1. INTRODUCTION

In the past decades, solar collectors have become an efficient, economical and popular way to produce clean and low-cost energy. Radiative energy from the sun can be converted into electricity with photovoltaic modules and/or into heat with solar thermal collectors. The latter mainly consist in a solar receiver component in which a heat transfer fluid flows to extract and transfer the produced heat. This receiver is mainly based on an absorber component (e.g. dark tube or plate), solar radiation being either directly received by this absorber or first concentrated by mirrors. In some cases, complementary components are added to the receiver to protect and thermally insulate the absorber (e.g. glass tube or glazing). With many different technologies available today, these solar thermal collectors (i.e., receivers with optional concentrating mirrors) can perform at low temperature for hot water production, medium temperature for steam generation or air conditioning, or high temperature for electricity production [1], [2]. All

technologies involve a radiative (solar) to thermal energy conversion, which means there is a need to both increase the absorbed incident solar flux and decrease the thermal losses. If vacuum receivers can reduce or cancel convective and conductive thermal losses using an evacuated glass tube or glazing around the absorber, specific coatings have been designed for reducing the emitted radiative flux of the hot absorber while increasing the absorbed solar flux [3]. This concept of solar selective absorber coating (SSAC) is very effective and innovative, performing and resistant coatings have been developed for many years by academic and industrial actors, leading to several commercial products [4–8].

Hundreds of publications are available on the subject of solar selective absorber coatings, a large majority of which focuses on practical studies about real materials, deposited with different techniques (sputtering, electro-deposition, paint, sol-gel, etc.), characterized using different methods and tested for specific purposes (optical efficiency, thermal stability, etc.). To estimate the optical performances most of these studies, and industrial catalogues, use two reference values: solar absorptance and thermal emittance. They are respectively the capacity of a component to absorb the incident solar flux density, and its capacity to lose thermal power by radiation. It is possible to join them in the solar-to-heat conversion efficiency, or heliothermal efficiency R_h, which is the ratio of the absorbed solar flux minus radiative thermal losses, over the incident concentrated solar flux. This heliothermal efficiency is more representative of the behavior of the solar collector, but introduces other specific parameters. Indeed, to calculate the heliothermal efficiency, it is necessary to choose: the collector geometry, imposing its concentration ratio C; the temperature of the heat transfer fluid inside the absorber, fixing the absorber temperature T_A; the location of the collector, which can have an impact on other parameters such as solar irradiation, cosine factor, ambient temperature T_0, etc.

Despite the relevance of the heliothermal efficiency as target value in solar thermal collector optimization, it is mostly not considered because these different parameters are missing [4], [5], [9]. For this reason, most selective coatings are strictly designed to achieve high solar absorptance and low emittance at high temperature, not necessarily to achieve high heliothermal efficiency [10], [11], [12]. Of course, high solar absorptance and low thermal emittance provide high heliothermal efficiency, but it does not automatically follow that this efficiency is maximized, as we will show in the following. Also, it can be difficult to compare the performance of selective coatings found in the literature, because their thermal emittance is not calculated at the same temperature, or when their heliothermal efficiency is calculated, it is not at the same concentration ratio.

We propose here a theoretical study on the optimization of spectrally selective coatings in terms of maximizing the heliothermal efficiency of solar collectors considering a wide range of absorber temperatures T_A (50 - 600 °C = 323 - 873 K) and concentration ratios C (10 - 300 suns). These values cover most existing solar thermal collectors with concentration, including the current generation of solar coatings (not stable in air at high temperature) and the next generation (stable in air up to 600 - 700 °C) [13]. They also correspond to the different collectors technologies available today, from linear Fresnel (low 2D concentration) to solar towers (high 3D concentration).

The example of a W/W-Al_2O_3/Al_2O_3 selective stack, comprising of a metallic infrared reflective sublayer (W), a cermet absorber layer (ceramic-metal composite, W-Al_2O_3) and an antireflective top layer (Al_2O_3), will be used as an illustration [4], [5], [7]. This type of design provides a refractive index gradient from support material (metallic alloy with high n) to the ambient (n = 1)

to capture incident light, by optimizing the layer thicknesses and metal volume fraction in the cermet [14]. W/W-Al_2O_3/Al_2O_3 coatings show good thermal stability in the considered temperature range (up to 600 °C), typically at 400°C in air and 580°C in vacuum [15], [16], [17]. Thermal stability can be further improved, as demonstrated by Cao et al. with WNi-Al_2O_3 cermet-based coatings [18].
Even though in practice the materials used can be varied depending on working conditions (particularly temperature and atmosphere), this W/W-Al_2O_3/Al_2O_3 SSAC design is representative of the ones used in most CSP applications today. Very similar results were obtained with other cermet-based coatings, such as the next generation of solar coatings (Mo-SiO_2 double cermet, Al_xO_y-AlN_x-Al) [11]. Likewise, analogous conclusions could be drawn in the case of next generation high temperature air-stable SSACs with tandem absorbers based on transition metal nitrides/oxides/carbides/oxynitrides [11]. Indeed in that case, a refractive index gradient is also sought for and obtained by varying the composition of the absorber materials (typically their atomic contents in nitrogen, carbon and oxygen).

From the complex spectral refractive indices of the SSAC materials, the spectral reflectance of the stack was calculated to estimate the optical performance. The coating parameters, i.e., the thickness of each layer and the composition (metal volume fraction) of the composite layer, were optimized so as to maximize heliothermal efficiency, using an in-house optimization algorithm.
With this optimization method, we present here, for the aforementioned large range of concentration ratios and absorber temperatures: the maximum attainable heliothermal efficiencies using an optimized W/W-Al_2O_3/Al_2O_3 selective coating (here chosen as an example); the corresponding optimal solar absorptance and thermal emittance, which to ensure maximum heliothermal efficiency, are not necessarily the highest and lowest possible, respectively; the optimized structures (layer thicknesses and composition) of the selective coatings in said (C, T_A) operating conditions, that provide such optimal heliothermal efficiency, and how they do so; the sensitivity of heliothermal efficiency and tolerance on coating parameters; the impact of using coatings optimized for other conditions than the ones they are used in. Originally, through a heliothermal efficiency 3D mapping vs. (C, T_A), we provide an all-in-one answer to typical interrogations of SSACs developers: what is the typical range of layer thicknesses, how to optically optimize the coating for high temperature, how to select the proper solar absorptance/thermal emittance ratio for mid temperatures, etc. By showing a 2D mapping of the heliothermal efficiency we provide a simple solution to compare different coatings to one another.
All this will allow us to alert selective coating developers and manufacturers, and give recommendations to help them obtain coatings both more efficient and more adapted to their future application.

2. THEORETICAL BACKGROUND AND SIMULATION DETAILS

2.1. Spectrally selective coating architecture

Figure 1 gives a schematic representation of the architecture of the spectrally selective coating studied in this paper. This spectrally selective absorber is based on a cermet, which is a mixture of a dielectric (ceramic) matrix (purple in Figure 1) and metal particle inclusions (black dots) [7]. Cermet-based spectrally selective coatings have been studied in the literature and used in

industries for decades [5], [7], [10]. When integrated in a multilayer coating with a dielectric antireflective layer (in blue) above and an infrared-reflective layer (in gray) below, such stack can create a very effective spectrally selective coating for thermal solar absorbers [5], [15]: the dielectric antireflective layer reduces solar reflection, thus increasing absorptance; the cermet layer provides high solar absorptance and low thermal emittance; the metallic layer is an infrared reflector which further reduces thermal emittance [6], [19], [16].

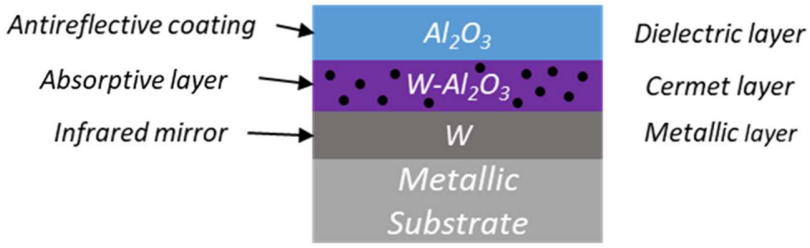

Figure 1 : Cermet-based spectrally selective coating architecture made of W,W-Al_2O_3 and Al_2O_3 multilayer stack on an iron substrate.

As an example, we have selected two materials: tungsten (W) for the infrared reflector and metallic inclusions in the cermet, and aluminum oxide (Al_2O_3) for the antireflective layer and matrix ceramic for the W-Al_2O_3 cermet [4], [8], [10]. They are put together to create a W/W-Al_2O_3/Al_2O_3 stack, known as a good spectrally selective coating with high heliothermal efficiency and good thermal stability (stability 400°C in air and 580°C in vacuum have been reported) [15], [16], [17]. Also, this type of architecture has been used in commercialized solar absorber coatings [17], [20]. A double cermet structure with a gradient of metallic content has even better efficiency [8], [10], [21]. In this paper a single cermet structure was chosen to reduce calculation times.
Several other similar structures with different constitutive materials were also tested, such as W/W-SiCH/SiCH [22], Mo/Mo-SiO_2/SiO_2 [23], [24], [25],W/W-AlN/AlN [26], [27], Pt-Al_2O_3 [21] or WTi-Al_2O_3 [14]. These results are not presented here, as they show the same general trends than for the representative example of W/W-Al_2O_3/Al_2O_3.
Finally, despite the fact that thermal absorbers are made of stainless steel [3], [28], iron (Fe) was selected as substrate, since it is the main component of steel, and no consensual data for steel was found in optical databases. Its thickness was fixed to 1 mm.

2.2. Spectral optical properties

Spectral reflectance $R(\lambda)$ can be calculated using a conventional method based on Fresnel equations, known as the Transfer Matrix Method (TMM), detailed in the literature [29], [30]. The stack presents four optical interfaces with their own reflection and transmission behavior. The interface characteristic matrix depends on the impact angle and wavelength λ of the incident light, and the thicknesses and spectral complex refractive indices $N(\lambda) = n(\lambda) + \mathbf{i}\square k(\lambda)$ of the layers on each side of the interface. $N(\lambda)$ depends on the nature and composition of the layer constitutive material. These matrices are multiplied in sequence to calculate the total power reflected and transmitted by the stack.

According to the conservation of energy, a radiation of wavelength λ incident on a material is either reflected, transmitted or absorbed. As the substrate of the stack is 1 millimeter-thick iron, its transmittance is zero. Its spectral absorptance $A(\lambda)$ is therefore $A(\lambda) = 1 - R(\lambda)$. Also, the relationship between spectral absorptance $A(\lambda)$ and spectral emittance $E(\lambda)$ at a specific wavelength λ, temperature T and angle θ is given by Kirchhoff's law of radiation: $A(\lambda, T, \theta) = E(\lambda, T, \theta)$. Thus $E(\lambda) = 1 - R(\lambda)$, and both $A(\lambda)$ and $E(\lambda)$ can be deduced from $R(\lambda)$.

2.3. Materials spectral complex refractive indices

To calculate $R(\lambda)$, $A(\lambda)$ and $E(\lambda)$, the spectral complex refractive indices of the stack constitutive materials (Figure 1) are needed. They were found in the literature: for Al_2O_3, from Boidin et al. [31]; for W, from Rakic et al. [32]; for Fe, from M. R. Querry [33]. These particular studies were selected because they cover a large spectral domain, from the solar range 280 – 4000 nm, to the IR range (for radiative losses calculation). They also present a good accuracy in the solar range, needed for a good estimation of solar performance [34]. Also, the data was measured on actual thin film samples fabricated by deposition techniques similar to that used in CSP industries. The data was linearly interpolated with a wavelength step of 5 nm.

The spectral complex refractive indices of the W-Al_2O_3 composite layer (Figure 1) were estimated by applying an Effective Medium Approximation (EMA) method [35]. Such methods consider a macroscopically inhomogeneous medium where quantities such as the dielectric function vary in space [36]. Different EMA theories have been reported in the literature, such as Bruggeman and Maxwell-Garnett [37].

Bruggeman theory was selected as no hypothesis of a major constituent is necessary and it allows simulating high volume fractions [37]. This theory has also been chosen in other studies [37], [38], [39]. At each wavelength, the complex dielectric function ε_{eff} of the cermet is deduced from that of the Al_2O_3 dielectric matrix ε_m and W metallic inclusions ε_i with a volume fraction of inclusions f (Eq. (1)). As a reminder, the complex dielectric function is directly linked to the complex refractive index as $\varepsilon(\lambda) = N(\lambda)^2$.

$$f\frac{\varepsilon_I - \varepsilon_{eff}}{\varepsilon_I + 2\varepsilon_{eff}} + (1-f)\frac{\varepsilon_M - \varepsilon_{eff}}{\varepsilon_M + 2\varepsilon_{eff}} = 0 \quad (1)$$

2.4. Optical performance

2.4.1. Solar absorptance

To evaluate the performance of a solar selective absorber, its solar absorptance A_S must be estimated. A_S represents the ratio of solar flux density (in W/m^2) absorbed by the absorber over the flux density the latter receives from the Sun (Eq. (2)) [5], [17]. The solar spectrum $J(\lambda)$ taken as a reference for calculation is the standard ASTM G173-03 Direct and Circumsolar (DC) AM1.5 spectrum, defined between 280 and 4000 nm with a step $d\lambda$ = 5 nm [34], [40], [41]. The absorbed solar flux density is deduced from spectral absorptance $A(\lambda) = 1 - R(\lambda)$, weighed by the solar spectrum $J(\lambda)$ and integrated over wavelength λ.

$$A_S = \frac{\int_{280\ nm}^{4000\ nm}[1-R(\lambda)]\cdot J(\lambda)\cdot d\lambda}{\int_{280\ nm}^{4000\ nm} J(\lambda)\cdot d\lambda} \quad (2)$$

2.4.2. Thermal emittance

The performance of a selective coating is also linked to its capacity to emit thermal radiation, which must be as low as possible. This capacity is illustrated by its thermal emittance $E_{BB}(T_A)$, which is the ratio of the irradiance emitted by the absorber at temperature T_A, compared to the irradiance of an ideal blackbody at the same temperature T_A [5], [17] (Eq. (3)). The largest spectral range available was considered for calculation.

$$E_{BB}(T_A) = \frac{\int_{280\ nm}^{30000\ nm}[1-R(\lambda)]\cdot L(\lambda,T_A)\cdot d\lambda}{\int_{280\ nm}^{30000\ nm} L(\lambda,T_A)\cdot d\lambda} \quad (3)$$

$L(\lambda, T_A)$ is Planck's law at T_A [42] given by Eq. (4) where λ is the wavelength (m), is the blackbody spectral irradiance (W/m²/m), T_A is the absorber temperature (K), h is Planck constant (J□s), c is the speed of light (m/s) and k is Boltzmann constant (J/K).

$$L(\lambda, T_A) = \frac{2\pi hc^2}{\lambda^5 \cdot e^{hc/(\lambda \cdot kT_A)} - 1} \quad (4)$$

The total irradiance (in W/m²) emitted by the blackbody at temperature T_A is given by the integration of Eq. (4) over wavelength (denominator in Eq. (3)). The total irradiance emitted by the absorber at T_A (numerator in Eq. (3)) is calculated by integrating over wavelength its spectral emittance $E(\lambda) = 1 - R(\lambda)$ weighed by the blackbody spectral irradiance at T_A (Eq. (4)). A large spectral domain from 280 nm to 30 μm was used to increase calculation accuracy [5], [35], [43].

2.4.3. Heliothermal efficiency

The heliothermal efficiency R_h quantifies the capacity of the absorber to convert incident solar radiation into heat, to be transferred to a heat transfer fluid. It is the ratio of absorbed solar flux density, minus the radiative thermal losses (due to the radiative exchange between the cold environment and the hot absorber, given by Stefan-Boltzmann law), divided by the total concentrated solar flux density received by the absorber [17], [22]. Convective and conductive thermal losses are also present for real thermal absorbers, but they are neglected here compared to much higher radiative losses (αT^4). R_h can be calculated from Eq. (5), where σ is the Stefan-Boltzmann constant. R_h depends on the absorber optical performance (A_S and $E_{BB}(T_A)$), the collector concentration ratio (C), the thermal absorber and ambient temperatures (respectively T_A and T_0), the solar irradiation ($I \approx 900$ W/m² for ASTM-G173 DC) and the concentrator (mirror) optical performance (η_{opt}). The optical performance of the concentrator η_{opt} represents an average value that includes several factors such as mirror solar reflectance, protective glass transmittance (if any), soiling of optical components, cosine and shadowing effects, etc. We selected a value $\eta_{opt} = 0.70$ from other studies [22].

$$R_h = A_S - \frac{E_{BB}\cdot\sigma(T_A^4 - T_0^4)}{C\cdot I\cdot\eta_{opt}} \quad (5)$$

Globally, the heliothermal efficiency represents the capacity for a coating to be a good candidate or a not for solar thermal conversion at high temperature ($T_A >> T_0$). R_h depends of solar absorptance A_S and thermal emittance $E_{BB}(T_A)$), which are both derived from spectral reflectance $R(\lambda)$. To ensure high heliothermal efficiency, the absorber must have a low spectral reflectance in the solar spectral domain (high absorptance) and a high reflectance in the infrared domain (low

emittance), with a radical change in reflectance at a cut-off wavelength, typically in the 1.5 - 2 µm range, i.e., it is spectrally selective.

2.5. Simulation and optimization method

Simulations were computed using a numerical code written on Scilab software [44]. The code can calculate spectral and total optical values of the W/W-Al_2O_3/Al_2O_3 stack (Figure 1) from spectral complex refractive indices, using the Transfer Matrix Method.
It also contains an optimization algorithm to optimize the composition of the cermet layer and thickness of each layer to achieve a suitable reflectance spectrum giving access to the maximal heliothermal conversion efficiency at specific operation conditions. The optimization target is the maximization of heliothermal efficiency R_h for different sets of parameters, i.e., concentration ratios C and absorber temperatures T_A. C was varied from 10 to 300 with a step of 10. T_A was comprised between 323 and 873 K (50 - 600°C) with a step of 25 K. For each set of parameters, the algorithm optimizes a set of four variables of the W/W-Al_2O_3/Al_2O_3 stack, which are the three layer thicknesses (W, W-Al_2O_3 and Al_2O_3) and the W-Al_2O_3 cermet volume fraction of W inclusions.
All layer thicknesses were allowed to vary between 0 and 200 nm, and the cermet volume fraction between 0 and 100%, to find the best coating solution (the best reflectance curve for obtain the highest heliothermal efficiency) in these domains. Stacks are randomly generated within this initial feasible set and the best are selected to reduce the feasible set for the next iteration. The optimization process stops when the standard deviation for the heliothermal efficiencies of the random stacks is lower than 10^{-7}. It means that for the last iteration the generated stacks must have the same heliothermal efficiency in % with a tolerance of 0.00001%.

3. RESULTS AND DISCUSSION

3.1. Optimized coating variables and optical performance vs. C and T_A

The selective coating was optimized to achieve the highest heliothermal efficiency for different sets of absorber temperatures T_A and concentration ratios C. The obtained maximum optical performance, i.e., heliothermal efficiencies R_h, and the corresponding solar absorptance A_S and thermal emittances $E_{BB}(T_A)$, are shown in Figure 2, Figure 3(a) and Figure 3(b) respectively. The heliothermal efficiency curve (Figure 2) is very smooth, which means that the optimization process performs well. The optimized coating variables, i.e., layer thicknesses and composition, that give rise to such optical performance, can be seen in Figure 4 and Figure 5. Figure 4 shows the optimized thickness ((a), in nm) and volume fraction of W inclusions (b) of the W-Al_2O_3 cermet absorber layer. Figure 5 shows the optimized thickness of the two other layers: the Al_2O_3 antireflective layer on top of the stack (a), and the IR-reflective W bottom layer (b). The former reduces solar reflection to further improve solar absorption, the latter reduces thermal emittance by providing high IR reflectance.
In all cases, three different regions can be observed, depending on the absorber temperature and concentration ratio. Each area is separated from the others by a clear break on the curves.

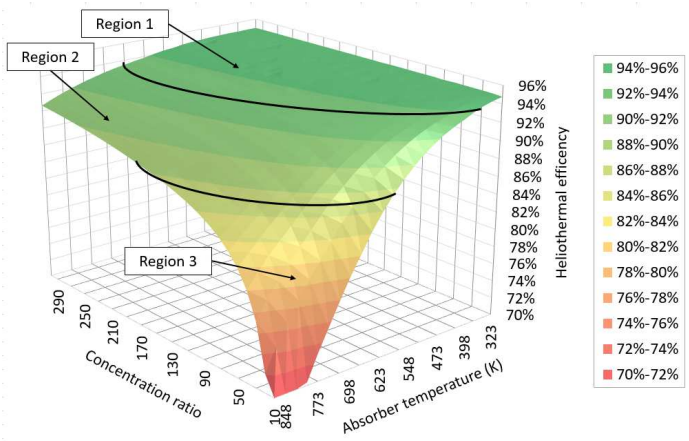

Figure 2 : Heliothermal efficiency of a selective coating optimized for different concentration ratios and absorber temperatures, example of W/W-Al_2O_3/Al_2O_3

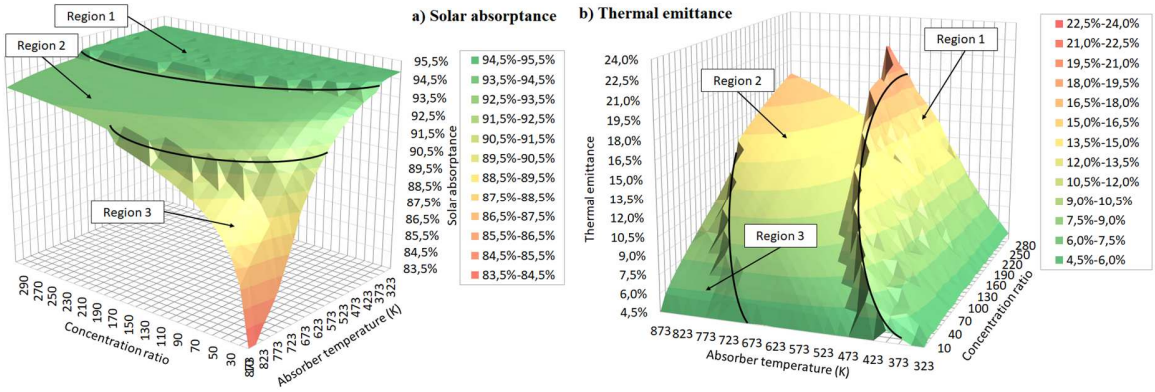

Figure 3: Solar absorptance (a) and thermal emittance (b) of a selective coating optimized to achieve the highest heliothermal efficiency for different concentration ratios and absorber temperatures, example of W/W-Al_2O_3/Al_2O_3

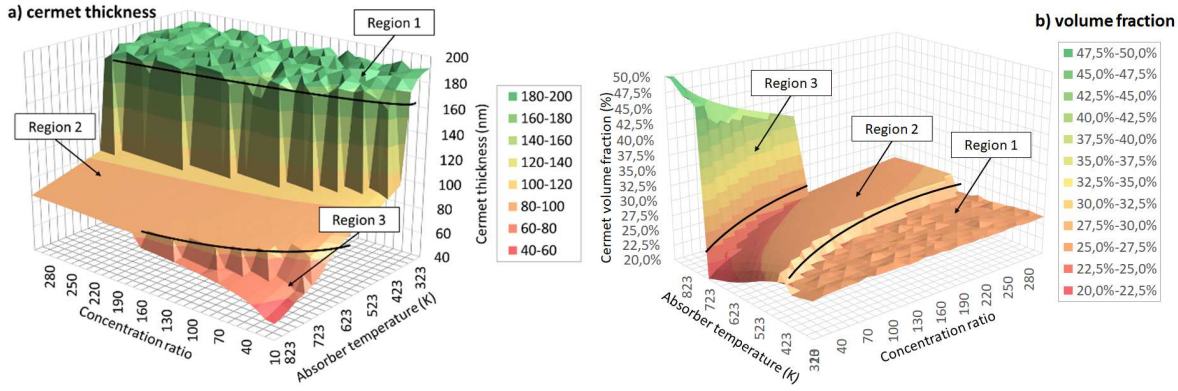

Figure 4 : Optimized W-Al_2O_3 cermet thickness (a) and W volume fraction (b) vs. concentration ratio and absorber temperature

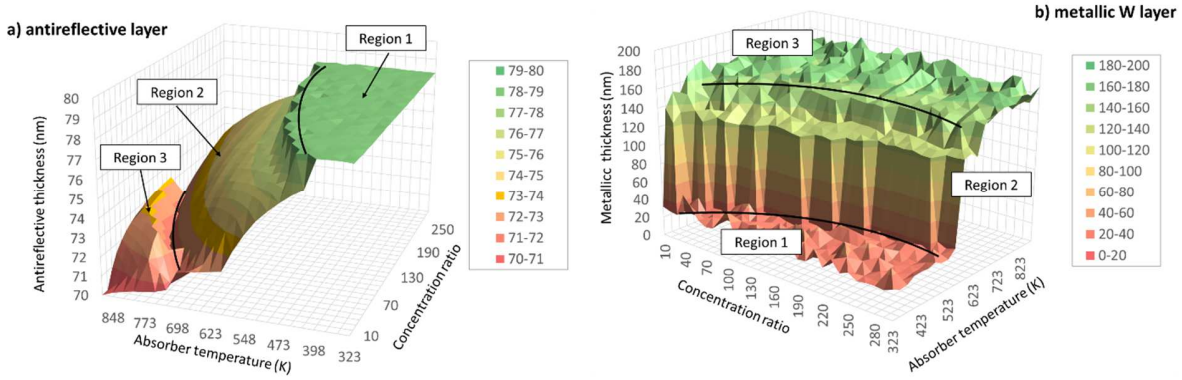

Figure 5 : Optimized thicknesses of Al_2O_3 antireflective layer (a) and IR-reflective metallic W bottom layer (b) vs. concentration ratio and absorber temperature

3.1.1. Region 1: [50°C < T_A < 200°C; 10 < C < 300]

A first region is observed at the lowest temperatures (T_A < 200°C, 473 K), whatever the concentration ratio in the studied range (10 < C < 300). Applications in this temperature range concern low temperature solar thermal, e.g., to produce residential hot water, heating and air conditioning, steam for industrial processes, etc. Temperature is not high enough for electricity production (steam turbines).

The highest heliothermal efficiency (Figure 2) is obtained there, especially at higher C. This tendency can easily be explained by analyzing Eq. (5). Indeed, a low absorber temperature T_A limits radiative losses (as given by Stefan-Boltzmann law), decreasing the fraction numerator and increasing the heliothermal efficiency. In the meantime, a high concentration ratio increases the concentrated solar flux density, increasing the denominator of the fraction and further lowering the impact of radiative losses on R_h.

This high heliothermal efficiency is obtained by prioritizing a high solar absorptance A_S = 93 - 95% (Figure 3(a)). In the meantime, thermal emittance $E_{BB}(T_A)$ (Figure 3(b)) is allowed to vary greatly with temperature, from 4% to 24% between 323 and 473 K, whatever C. Therefore thermal emittance has a very low influence on heliothermal efficiency in this region. It is linked to the fact that the values of σT_A^4 remain low in any case, so even a higher value of $E_{BB}(T_A)$ does not affect much the heliothermal efficiency (Eq. (5)).

To shed better light into this matter, the reflectance spectra of two coatings optimized for region 1 at [coating 1: C = 30, T_A = 100°C = 373 K] and [coating 2: C = 60, T_A = 200°C = 473 K] are shown in Figure 6. Optimal $R(\lambda)$ is low from 0.28 to 4 µm then increases quickly at higher wavelengths. During the optimization, a choice must be made between high $A(\lambda)$ and low $E(\lambda)$ at a given wavelength (due to Kirchhoff's law of radiation). Thus $R(\lambda)$ is minimized, i.e., $A(\lambda)$ is maximized over the whole solar range, up to 4 µm, to prioritize high A_S. Beyond the solar range, $R(\lambda)$ is then allowed to quickly increase again, so as to reduce $E(\lambda)$ and $E_{BB}(T_A)$ (Eq.(3)). Thus for low absorber temperatures, the optimization indeed prioritizes A_S over low $E_{BB}(T_A)$, but in a second step also minimizes the latter insofar as possible.

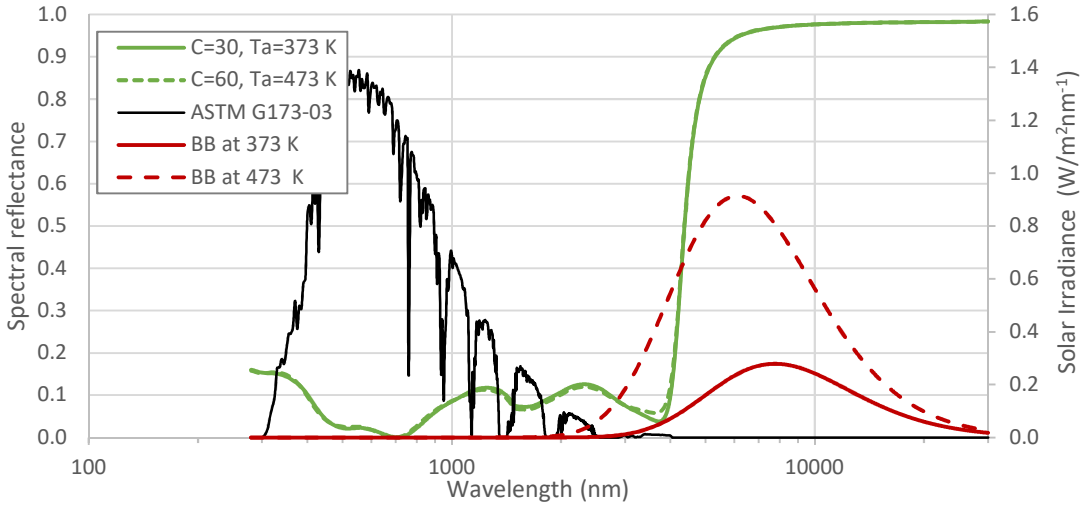

Figure 6 : Spectral reflectance (green) of two coatings optimized for two typical (C, T_A) in region 1, compared to solar (black) and blackbody (red) spectra

Table 1 gives the optimal structure and performance of the two coatings shown in Figure 6. Despite the varying operating conditions (C, T_A), both coatings are very similar in terms of their structure and composition, and subsequent spectral reflectance (Figure 6). Their solar absorptance is the same, due to similar cermet absorber layers. Their thermal emittance $E_{BB}(T_A)$ is different (6.2% for coating 1, 11.3% for coating 2), but this is mostly because of the differing position of the blackbody emission with temperature, considered in the calculation of $E_{BB}(T_A)$ (expression (3)): for coating 1 at T_A = 373 K (solid lines), most of the emitted radiation is avoided as it happens almost entirely in the high reflectance region, resulting in lower thermal emittance; while for coating 2 at T_A = 473 K (dashed lines), a larger part of the blackbody emission happens before the switch to high reflectance, resulting in higher thermal emittance. This difference in $E_{BB}(T_A)$ has low incidence on the corresponding optimal heliothermal efficiency (-0.5%) because $E_{BB}(T_A)$ itself has low incidence, as previously discussed.

Overall, in region 1 optimal coatings are similar. For the W-Al_2O_3 cermet absorber layer (Figure 4), the optimal volume fraction remains close to 26%, while the optimal layer thickness is between 180 and 200 nm. This thickness optimum is close to the maximum of the initial range allowed by the optimization process (0 - 200 nm). To ensure that the optimum was indeed comprised in this initial range, optimizations with maximum cermet thickness of 500 nm instead of 200 nm were also carried out, but the optimum remained in the 180 - 200 nm range. A thicker absorber would guarantee even higher solar absorptance, but would also increase thermal emittance and eventually decrease heliothermal efficiency.

Table 1 : Description and optical performance of optimized W/W-Al_2O_3/Al_2O_3 selective coatings in region 1 [50°C < T_A < 200°C; 10 < C < 300], region 3 [400°C < T_A < 600°C; 10 < C < 80] and region 2 [200°C < T_A < 400°C; 80 < C < 300]

Region	Coating	Layer thicknesses	Volume fraction	Conditions of use	Optical performance

		W	W-Al_2O_3	Al_2O_3	W-Al_2O_3	C	T_A (K)	A_S	$E_{BB}(T_A)$	R_h
1	1	136 nm	189 nm	78 nm	25.5%	30	373	*94.9%*	*6.2%*	*94.7%*
	2	139 nm	184 nm	78 nm	25.5%	60	473	*94.9%*	*11.3%*	*94.1%*
3	3	166 nm	71 nm	73 nm	41.6%	80	823	*91.4%*	*9.0%*	*86.8%*
	4	185 nm	52 nm	40 nm	66.0%	10	873	*82.3%*	*4.5%*	*59.4%*
2	5	160 nm	100 nm	76 nm	25.9%	20	523	*94.1%*	*7.6%*	*92.7%*
	6	146 nm	89 nm	74 nm	26.7%	250	823	*93.9%*	*16.6%*	*91.2%*

On the whole the optimal Al_2O_3 antireflective thickness (Figure 5) does not change very much in the whole studied domain, between 70 and 80 nm. This evolution is to be put in regard to that of the optimal cermet volume fraction (Figure 4(b)). The latter is directly correlated to the cermet refractive index n_{cermet} (see section 2.3). As a quick reminder, to create an antireflective single layer (AR), its refractive index must be $n_{AR} \approx \sqrt{n_{cermet}}$ and its thickness must be $d_{AR} \propto \lambda_0/4\, n_{AR}$ to generate a destructive interference at wavelength λ_0 [29]. Mostly the cermet volume fraction/refractive index does not vary significantly in the overall domain (Figure 4). Therefore the thickness of the AR layer remains close to its optimal value whatever the conditions. In region 1, the optimal thickness is around 78 - 80 nm.

Concerning the W infrared-reflective layer, overall the curve area in Figure 5 is not very smooth, despite the fact that heliothermal efficiency standard deviation after optimization is very small ($< 10^{-7}$). It means that the metallic layer has less impact on heliothermal efficiency than the other layers, and differences of a few nanometers on the metallic layer thickness can ensure similar values of R_h. W layer optimal thickness is low in region 1, between 20 and 60 nm, since thermal emittance is not critical in this domain.

3.1.2. Region 3: [400°C < T_A < 600°C; 10 < C < 80]

The lowest heliothermal efficiencies (below 85%) are obtained for low concentration ratios and high absorber temperatures (Figure 2). Some of these conditions can be hard to achieve experimentally, especially to reach high T_A at low C. Conditions such as [C = 50, T_A = 500°C = 773 K] are however envisaged for linear Fresnel reflectors with a secondary concentrator and a preheating solar field stage [45].

In this region, a quick decrease of both solar absorptance and thermal emittance is observed (Figure 3). T_A and subsequent blackbody emission are high, therefore to reduce radiative losses and achieve high heliothermal efficiency, the optimization process focuses on lowering thermal emittance E_{BB}. To do so, spectral emittance $E(\lambda)$ is decreased in the overall blackbody emission range, as illustrated by Figure 7. The latter shows the reflectance spectra of two coatings optimized for region 3, [coating 3: C = 80, T_A = 550°C = 823 K] and [coating 4: C = 10, T_A = 600°C = 873 K]. As temperature increases, the blackbody spectrum is shifted towards lower wavelengths and its overlap with the solar spectrum increases. Consequently the optimization also decreases spectral absorptance $A(\lambda) = E(\lambda)$ in some part of the solar spectrum, thus decreasing solar absorptance. The latter is no longer a priority to increase R_h, especially since concentration is low and the amount of incident solar flux, and subsequent absorbed solar flux, are low anyway. In this region, the optimization prioritizes minimizing the losses over maximizing the solar input. This drastic change in behavior confirms why it is hard to provide good heliothermal conversion in this range of operating conditions (high T_A at low C). The

extreme cases of lowest C (10) combined with highest T_A (600°C) are even physically impossible.

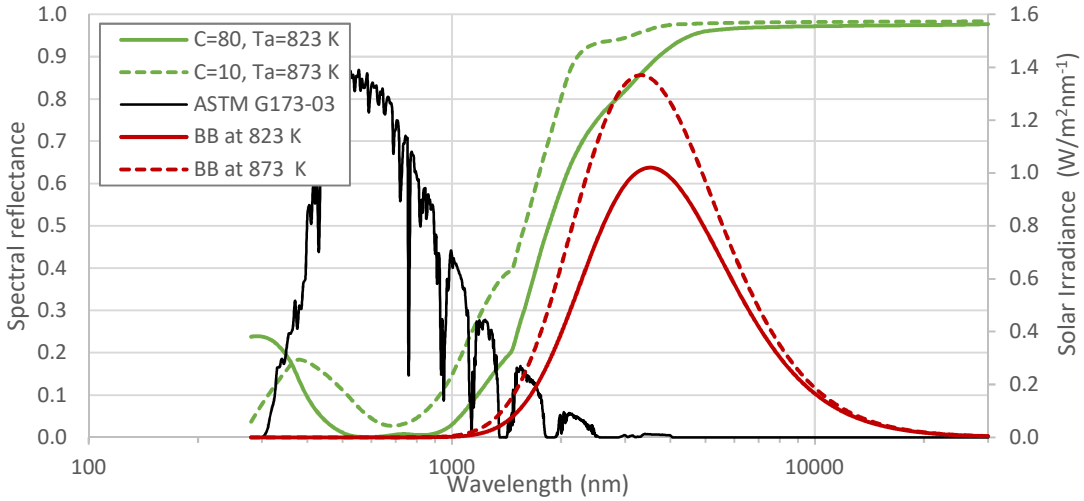

Figure 7 : Spectral reflectance of two coatings optimized for typical (C, T_A) in region 3, compared to solar and blackbody spectra

Table 1 shows the composition and the optical performance for coatings 3 and 4 optimized for region 3. Overall in this region, to achieve low E_{BB}, IR-reflective W optimal thickness increases to 160 - 180 nm (Figure 5). Meanwhile, the cermet thickness decreases to 40 - 80 nm while the volume fraction of W inclusions increases quickly up to 50% (Figure 4). Thus the cermet becomes thin with a high metallic content, so that its optical behavior tends towards that of an IR reflective - low emissive material, like the W layer underneath, to further decrease thermal emittance. Heliothermal efficiency R_h is poor (lower than 90%) in all cases. However this kind of low absorptive/emissive coating can be useful to coat the parts that are not exposed to the concentrated solar irradiance, where good absorption is less imperative, simply to reduce radiative losses. It can thus be used to coat absorber tubes extremities, or the side of the absorber exposed to the direct (not concentrated) solar flux.

3.1.3. Region 2: [200°C < T_A < 400°C; 80 < C < 300]

This region corresponds to intermediate absorber temperatures and concentration ratios, typical of solar thermal electricity technologies, such as parabolic troughs using steam or synthetic oil as heat transfer fluid.

Heliothermal efficiency is in the intermediate range of 85 - 93% (Figure 2). Its maximization calls for a compromise between high solar absorptance and low thermal emittance (Figure 3). Solar absorptance (A_S = 90 - 94%) is allowed to be slightly lower than in region 1 but much higher than in region 3. It is more dependent on both concentration ratio and absorber temperature than in region 1. Thermal emittance ($E_{BB}(T_A)$ = 4 - 18%) varies, less than in region 1 but more than in region 3.

Meanwhile, a drastic drop of optimal W-Al_2O_3 cermet thickness and a small jump in volume fraction are observed compared to region 1 (Figure 4). The cermet optimized thickness and volume fraction vary slightly more than in region 1, between 80 and 100 nm and from 22 and

30%, respectively. Meanwhile, the optimal thickness of the Al_2O_3 antireflective layer slowly decreases from 78 to 72 nm (Figure 5(a)), as the cermet volume fraction of metallic inclusions increases, i.e., as n_{cermet} increases (since the refractive index of W inclusions is higher than that of Al_2O_3 matrix). As in this region low thermal emittance is also relevant to the maximization of R_h, the W layer optimal thickness increases to 120 - 140 nm compared to region 1 (Figure 5(b)).
Figure 8 illustrates the reflectance spectra of two coatings optimized in region 2 for two different sets of operational conditions: [coating 5: C = 20, T_A = 250°C = 523K] and [coating 6: C = 250, T_A = 550°C = 823K]. Despite the large differences in operational conditions, the two spectra are quite similar up to 2 µm, with a typical "W" shape in the solar region. This results in very close solar absorptance values (Table 1). Beyond 2 µm, $R(\lambda)$ increases differently, to adjust thermal emittance $E_{BB}(T_A)$ to the blackbody spectra at the two different absorber temperatures. The hotter the absorber/blackbody, the steeper the reflectance increase. The transition wavelength λ_c is around 2.5 µm for coating 5 and 2.8 µm for coating 6, which ensure a large portion of absorbed solar power. For coating 6, the higher concentration ratio of 250 makes more profitable for the heliothermal efficiency to absorb solar radiation between 1.5 and 2.8 µm than not to emit in this region: high C gives a high absorbed solar flux that better compensates for the higher radiative losses (Eq.(5)). To ensure this result and adapt to the different (C, T_A) conditions, the two optimal coatings are dissimilar (Table 1). At higher C and T_A (coating 6), the cermet absorber and W IR-reflective layers are thinner, giving lower solar absorptance and allowing for higher thermal emittance.

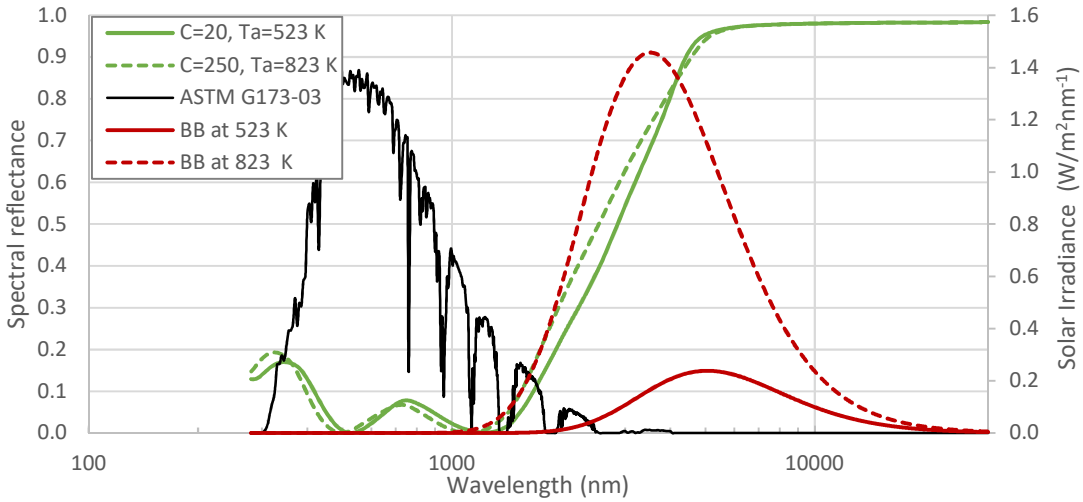

Figure 8 : Spectral reflectance of two coatings optimized for typical (C, T_A) in region 2, compared to solar and blackbody spectra

Overall, in this region all coating parameters evolve to adapt to the operating conditions, in order to maximize heliothermal efficiency. Each selective coating optimized in this region is different from all others. This behavior indicates that in this intermediate region the solar selective absorber coating should be specifically designed to adapt to the solar thermal collector technology (and related operating conditions) it will be used for.

3.2. Impact on optical performance of using a selective coating optimized for other (C, T_A) operating conditions

Given the existence of these different modes of optimization, and especially of region 2 where every set (C, T_A) of operating conditions calls for a different optimal selective coating, the need arises to evaluate the impact on optical performance of using a selective coating that was not optimized for the actual operating conditions of the aimed application.
For this purpose, as an example, two W/W-Al_2O_3/Al_2O_3 stacks optimized for different values of C and T_A were selected. Coating 1 was optimized for [C = 30, T_A = 100°C = 373 K] in region 1 (see section 3.1.1). It is representative of a coating designed for low temperature solar thermal applications. Coating 3 was optimized for [C = 80, T_A = 550°C = 823 K] in region 3 (see section 3.1.2). Because this point is very close to region 2, the heliothermal efficiency is still good (up to 85%). It illustrates the case of a high temperature selective coating for parabolic trough vacuum receiver tubes [15]. Table 2 recalls the full description and optical performance of the two optimized coatings. For each coating, its optical performance was evaluated at optimal C and T_A (the ones the coating was optimized for) and at non-optimal C and T_A (the ones the other coating was optimized for).

Table 2 : Description and optical performance of two optimized W/W-Al_2O_3/Al_2O_3 selective coatings, at optimal and non-optimal C and T_A

Region	Coating	Layer thicknesses			Volume fraction	Conditions of use			Optical performance		
		W	*W-Al_2O_3*	*Al_2O_3*	*W-Al_2O_3*	*Optimal*	*C*	*T_A (K)*	*A_S*	*$E_{BB}(T_A)$*	*R_h*
1	1	136 nm	189 nm	78 nm	25.5%	Yes	30	373	94.9 %	6.2 %	94.7 %
						No	*80*	*823*	*94.9 %*	*42.4%*	*73.4 %*
3	3	166 nm	71 nm	73 nm	41.6 %	*No*	*30*	*373*	*91.4 %*	*3.0%*	*91.6%*
						Yes	80	823	91.4 %	9.0 %	86.8 %

As solar absorbance A_s only depends on the coating structure (layer thicknesses and refractive indices), for a given coating it remains constant whatever its conditions of use. Thermal emittance $E_{BB}(T_A)$ however also depends on temperature, as it is established from the blackbody irradiance spectrum (Eq. (3) and (4)). Therefore, for each coating $E_{BB}(T_A)$ changes with the conditions of use: it increases with temperature. $E_{BB}(T_A)$ of coatings 1 and 2 respectively vary from 6.2 to 42.4% and from 3 to 9% when T_A increases from 373 to 823 K. The spectral reflectance of the two coatings explains these differences in the evolution of their $E_{BB}(T_A)$. For coating 1 (Figure 6, solid green line), reflectance is low below 4 µm to ensure solar absorptance as high as possible. Therefore when T_A increases and the blackbody spectrum is shifted towards lower wavelengths, the coating becomes highly emissive. Whereas coating 2 is optimized for the higher temperature of 823 K, thus its spectral reflectance (Figure 7) is low in the spectral range of the blackbody at 373 K, which occurs at higher wavelength. The evolution of its $E_{BB}(T_A)$ when increasing T_A is mostly due to the higher intensity of blackbody emission at 823 K.

As a consequence, if coating 3 optimized for [C = 80, T_A = 550°C = 823 K] (region 3) is used at non-optimal conditions [C = 30, T_A = 100°C = 373 K] (region 1), the heliothermal efficiency increases from 86.8% to 91.6%, due to lower temperature T_A and subsequent lower thermal emittance $E_{BB}(T_A)$ and radiative losses $E_{BB}(T_A) \sigma T_A^4$. This type of non-optimal utilization, i.e., a

coating optimized for higher T_A used at much lower T_A is efficient. However R_h = 94.7% (+3.1%) can be reached with a coating optimized for these "lower" conditions, so it is still more efficient to use an optimized coating.
In an opposite manner, R_h is reduced from 94.7% to 73.4% when using coating 1 at higher temperature and concentration, because of the strong increase in thermal emittance (from 6.2% to 42.4%). This type of non-optimal utilization, i.e., a coating optimized for lower T_A used at much higher T_A, must absolutely be avoided.

To further explore these questions, the heliothermal efficiency of the two coatings were calculated for all concentration ratios and absorber temperatures previously studied. The differences between efficiencies at optimal and non-optimal conditions are plotted in Figure 9. The black area corresponds to the optimal, i.e., the C and T_A couple for which the selective coating was optimized (Table 2). Outside this optimal area, heliothermal efficiency is necessarily lower, so the (non-optimal − optimal) difference is negative. Difference ranges are illustrated in four different colors. In green, the differences are between 0 and -0.5%. In this area, the coating performs well and it is not necessary to optimize it again. In blue, the differences are included between -0.5 and -2%. The coating performs with only a small loss in performance, but it can be further optimized. In orange, the differences are included between -2% and -20%. We recommend not to use this coating in these conditions and to switch to a coating specifically optimized for said conditions. In red, the difference is above 20% and the selective coating is not functional: heliothermal efficiency is null.

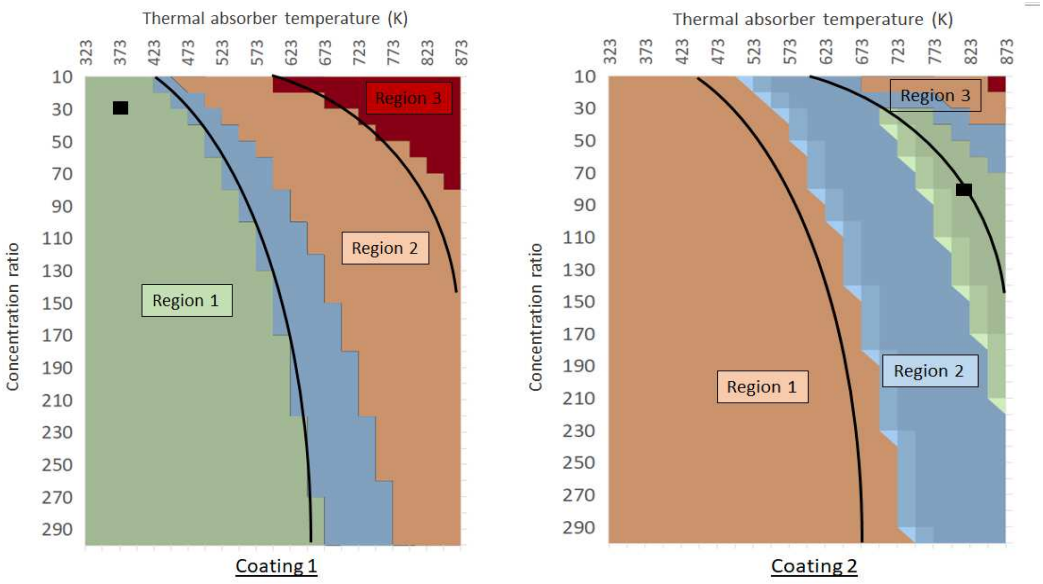

Figure 9 : Heliothermal efficiency loss between optimal (black) and non-optimal [C, T_A] conditions for the two coatings of Table 2

For coating 1 designed for [C = 30, T_A = 100°C = 373 K] (region 1) a large green area exists where the coating can also be very efficiently used. It includes all concentration ratios for absorber temperatures below 423 K (150°C), and extends to increasing temperatures for

increasing concentration ratios. This corresponds to region 1 and most of region 2. At high temperatures, especially for low concentration ratios, this coating is not applicable.
For coating 2 designed for [C = 80, T_A = 550°C = 823 K] (edge of region 3) the area of efficient use (green or blue) is more restricted. Apart from optimal conditions, this coating can also be used close to optimal temperature with lower concentration ratios, for instance at C = 50, that would represent linear Fresnel reflectors with a secondary concentrator. For lower temperatures and concentration ratios (orange area), this coating is still applicable but much less efficient, thus not recommended.

These observations and repartition in three regions is not specific to the chosen example of cermet-based design, but representative of most solar selective absorber coatings. Overall, coatings optimized for a specific condition in region 1 are applicable over a large range of (C, T_A), provided the latter conditions remain moderate. Coatings optimized for a specific condition in region 3 (high T_A, low C) must be used preferentially in this range, and in any case not at low T_A. Whatever the case may be, before using a selective coating in other conditions than the ones it was optimized for, we encourage calculating the resulting loss in heliothermal efficiency.

3.3. Sensitivity and tolerance on optimization variables

Finally, to study the relative sensitivity of the optimization process to its variables (layer thicknesses and cermet volume fraction in our example), the evolution of the standard deviation of each variable and of the optimization target (R_h) is presented in Figure 10 vs. the number of iterations of the optimization algorithm, for [C = 80, T_A = 350°C, 623 K]. Standard deviation is in nm for layer thicknesses and in % for the cermet volume fraction and heliothermal efficiency. Section 2.5 gives more details about the optimization process. Figure 10 shows that all standard deviations decreased as the number of iterations increased, meaning the optimization algorithm performs well and tends towards a solution. The optimization stops when R_h standard deviation is lower than 0.00001% for the 100 random stacks of the last iteration (20 in this example), giving a final reduced feasible set for all variables. The variable standard deviation is an image of the sensitivity and tolerance on each variable. The lower its standard deviation, the more reduced is the feasible set of the variable, the smaller the tolerance on its value.

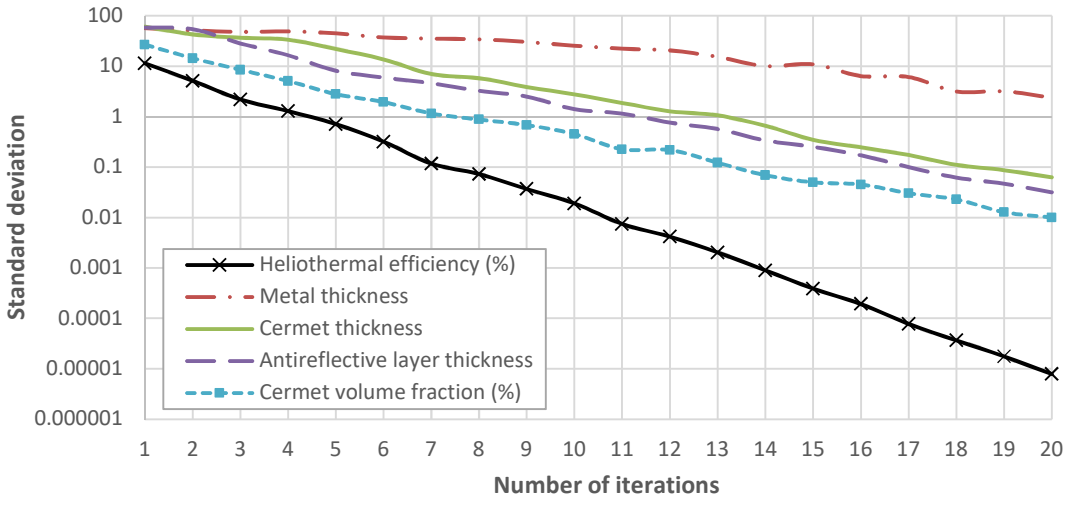

Figure 10 : Standard deviation of optimization target (heliothermal efficiency) and variables vs. number of iterations

Thus Figure 10 shows that the W-Al_2O_3 cermet volume fraction (dotted blue line), which drives the cermet absorber optical properties, and subsequent absorptive and emissive behavior, is the most critical variable and must be controlled accurately. The same sensitivity can be observed for other cermet-based selective coatings. Contrarily, the heliothermal efficiency is much less sensitive to the thickness of the IR-reflective W metal layer (dash-dot red line).
The knowledge of the sensitivity/tolerance on variables such as layer thicknesses and composition is very valuable for coating designers and manufacturers. Let us consider for instance that a manufacturer aims to produce large quantities of W/W-Al_2O_3/Al_2O_3 selective coatings (or another cermet-based coating) with a tolerance on their heliothermal efficiency of 0.01% (iteration 11 on Figure 10). In this case, the tolerances are low, within 0.2% for the W-Al_2O_3 cermet volume fraction, and within 1 nm and 2 nm for the antireflective and cermet layer thicknesses, respectively. These values are compatible with the level of control provided by most thin film deposition techniques, at least regarding thicknesses. As for the metal layer thickness, the tolerance is much larger, within 20 nm, without impacting the heliothermal efficiency.

4. CONCLUSION

In this paper a solar selective absorber coating was numerically optimized to study the impact of working conditions (absorber temperature T_A and concentration ratio C) on the coating optimal design that maximizes its optical performance, i.e. its heliothermal efficiency. As an example, a cermet-based W/W-Al_2O_3/Al_2O_3 solar selective absorber coating was considered. Such IR-reflective/absorptive/antireflective structure ensures high heliothermal efficiency by providing both high solar absorptance and low thermal emittance. Similar conclusions can be drawn for other types of SSACs, such as next-generation materials stable in air up to 600 – 700 °C [11], [43], [46]. Using an optimization algorithm, the stack was optimized so as to maximize its heliothermal efficiency (solar-to-heat conversion), by optimizing layer thicknesses and the metal volume fraction of the W-Al_2O_3 cermet. Optimization was performed for different sets of concentration ratios (C = 10 -300) and absorber temperatures (T_A = 323 - 873 K). Maps of maximal heliothermal efficiency and corresponding optimal variables vs. (C, T_A) were thus obtained, and recommendations for selective coatings manufacturers were given accordingly. In particular, the importance of considering the final (C, T_A) operating conditions when designing and optimizing such coatings, and of using said coatings in or near the conditions they were optimized for, were underlined. A coating optimized for low T_A must not be used at high T_A. A coating optimized for high T_A can efficiently be used at low T_A, but it will not be optimal. Efficient solar selective absorber coatings need not systematically be designed for a specific *set* of absorber temperature T_A and concentration ratio C, but then they should remain optimal for a specific *range* of absorber temperatures and concentration ratios, according to three different regions.
Indeed, three regions with distinct behaviors were identified, indicating that a universal selective coating cannot exist. For low absorber temperatures (T_A < 200°C (473 K)), independently of C between 10 and 300 (low temperature solar thermal applications), solar absorptance is the key physical quantity to maximize heliothermal efficiency. Indeed, thermal emittance is less crucial

since radiative losses are small at low T_A. Consequently, the optimal layer thicknesses and cermet composition are rather constant in this region. For high absorber temperatures and low concentration ratios (e.g. Linear Fresnel reflectors), heliothermal efficiency is strongly driven by thermal emittance and radiative losses. Solar absorptance must be lower to reduce thermal emittance, due to the overlap between solar and blackbody spectral radiations. This leads to lower efficiencies. For intermediate temperatures and concentration ratios, a radical change in the coating composition (thickness, volume fraction) between two close points is observed. In this region, it is necessary to optimize the selective coating for a specific C and T_A couple. Industrial catalogs may therefore systematically propose, for a given type of selective coating, at least three different options, corresponding to different solar thermal technologies and collector types: one optimized for low T_A, one for medium C and T_A and one for high T_A and low C.
Finally, developers and manufacturers should bear in mind that above other parameters such as layer thicknesses, the absorber chemical composition, strongly influencing its optical properties, is the most critical parameter and must be controlled very accurately to design an absorber coating with high heliothermal efficiency.

5. ACKNOWLEDGEMENTS

This work was supported by the French "Investments for the future" program managed by the National Agency for Research (ANR) under contract ANR-10-LABX-22-01-SOLSTICE.

6. REFERENCES

[1] H.L. Zhang, J. Baeyens, J. Degrève, G. Cacères, Concentrated solar power plants: Review and design methodology, Renewable and Sustainable Energy Reviews. 22 (2013) 466–481. https://doi.org/10.1016/j.rser.2013.01.032.

[2] Y. Tian, C.Y. Zhao, A review of solar collectors and thermal energy storage in solar thermal applications, Applied Energy. 104 (2013) 538–553. https://doi.org/10.1016/j.apenergy.2012.11.051.

[3] S.S. Kumar, K.M. Kumar, S.R.S. Kumar, Design of Evacuated Tube Solar Collector with Heat Pipe, Materials Today: Proceedings. 4 (2017) 12641–12646. https://doi.org/10.1016/j.matpr.2017.10.075.

[4] C. Atkinson, C.L. Sansom, H.J. Almond, C.P. Shaw, Coatings for concentrating solar systems - A review, Renewable and Sustainable Energy Reviews. 45 (2015) 113–122. https://doi.org/10.1016/j.rser.2015.01.015.

[5] C.E. Kennedy, Review of Mid- to High- Temperature Solar Selective Absorber Materials Review of Mid- to High- Temperature Solar Selective Absorber Materials, Technical Report NREL. (2002) 1–51.

[6] C.E. Kennedy, H. Price, Progress in Development of High-Temperature Solar Selective Coating, in: ASME 2005 International Solar Energy Conference, 2005: pp. 749–755. https://doi.org/10.1115/ISEC2005-76039.

[7] F. Cao, K. McEnaney, G. Chen, Z. Ren, A review of cermet-based spectrally selective solar absorbers, Energy and Environmental Science. 7 (2014) 1615–1627. https://doi.org/10.1039/c3ee43825b.

[8] C.H. Trease, H. Hadavinia, P.E. Barrington, Solar Selective Coatings : Industrial State-of-the-Art, (2013) 1–19. https://doi.org/10.2174/1874464811306010001.
[9] C.K. Ho, B.D. Iverson, Review of high-temperature central receiver designs for concentrating solar power, Renewable and Sustainable Energy Reviews. 29 (2014) 835–846. https://doi.org/10.1016/j.rser.2013.08.099.
[10] N. Selvakumar, H.C. Barshilia, Review of physical vapor deposited (PVD) spectrally selective coatings for mid- and high-temperature solar thermal applications, Solar Energy Materials and Solar Cells. 98 (2012) 1–23. https://doi.org/10.1016/j.solmat.2011.10.028.
[11] K. Xu, M. Du, L. Hao, J. Mi, Q. Yu, S. Li, A review of high-temperature selective absorbing coatings for solar thermal applications, Journal of Materiomics. 6 (2020) 167–182. https://doi.org/10.1016/j.jmat.2019.12.012.
[12] H. Wen, W. Wang, W. Wang, J. Su, T. Lei, C. Wang, Enhanced spectral absorption of bilayer WOx/SiO2 solar selective absorber coatings via low vacuum pre-annealing, Solar Energy Materials and Solar Cells. 202 (2019) 110152. https://doi.org/10.1016/j.solmat.2019.110152.
[13] Y. Li, C. Lin, D. Zhou, Y. An, D. Li, C. Chi, H. Huang, S. Yang, C.Y. Tso, C.Y.H. Chao, B. Huang, Scalable all-ceramic nanofilms as highly efficient and thermally stable selective solar absorbers, Nano Energy. 64 (2019). https://doi.org/10.1016/j.nanoen.2019.103947.
[14] X. Wang, J. Gao, H. Hu, H. Zhang, L. Liang, K. Javaid, F. Zhuge, H. Cao, L. Wang, High-temperature tolerance in WTi-Al2O3 cermet-based solar selective absorbing coatings with low thermal emissivity, Nano Energy. 37 (2017) 232–241. https://doi.org/10.1016/j.nanoen.2017.05.036.
[15] A. Antonaia, A. Castaldo, M.L. Addonizio, S. Esposito, Stability of W-Al2O3 cermet based solar coating for receiver tube operating at high temperature, Solar Energy Materials and Solar Cells. 94 (2010) 1604–1611. https://doi.org/10.1016/j.solmat.2010.04.080.
[16] L. Rebouta, A. Sousa, P. Capela, M. Andritschky, P. Santilli, A. Matilainen, Solar selective absorbers based on Al2O3 : W cermets and AlSiN / AlSiON layers, Solar Energy Materials and Solar Cells. 137 (2015) 93–100. https://doi.org/10.1016/j.solmat.2015.01.029.
[17] K. Zhang, L. Hao, M. Du, J. Mi, J.N. Wang, J. ping Meng, A review on thermal stability and high temperature induced ageing mechanisms of solar absorber coatings, Renewable and Sustainable Energy Reviews. 67 (2017) 1282–1299. https://doi.org/10.1016/j.rser.2016.09.083.
[18] F. Cao, D. Kraemer, T. Sun, Y. Lan, G. Chen, Z. Ren, Enhanced thermal stability of W-Ni-Al2O3 Cermet-based spectrally selective solar absorbers with tungsten infrared reflectors, Advanced Energy Materials. 5 (2015) 1–7. https://doi.org/10.1002/aenm.201401042.
[19] R.E. Peterson, J.W. Ramsey, Thin film coatings in solar−thermal power systems, Journal of Vacuum Science and Technology. 12 (1975) 174. https://doi.org/10.1116/1.568749.
[20] C. Wang, W. Li, Z. Li, B. Fang, Solar thermal harvesting based on self-doped nanocermet: Structural merits, design strategies and applications, Renewable and Sustainable Energy Reviews. 134 (2020) 110277. https://doi.org/10.1016/j.rser.2020.110277.
[21] Z.Y. Nuru, D.E. Motaung, K. Kaviyarasu, M. Maaza, Optimization and preparation of Pt - Al2O3 double cermet as selective solar absorber coatings, Journal of Alloys and Compounds. 664 (2016) 161–168. https://doi.org/10.1016/j.jallcom.2015.12.201.
[22] A. Soum-Glaude, I. Bousquet, L. Thomas, G. Flamant, Optical modeling of multilayered coatings based on SiC(N)H materials for their potential use as high-temperature solar

selective absorbers, Solar Energy Materials and Solar Cells. 117 (2013) 315–323. https://doi.org/10.1016/j.solmat.2013.06.030.
[23] J. Wang, B. Wei, Q. Wei, D. Li, Optical property and thermal stability of Mo/Mo-SiO2/SiO2 solar-selective coating prepared by magnestron sputtering, Physica Status Solid. 667 (2011) 664–667. https://doi.org/10.1002/pssa.201026301.
[24] R. Yang, J. Liu, L. Lin, Y. Qu, W. Zheng, Optical properties and thermal stability of colored solar selective absorbing coatings with double-layer antireflection coatings, Solar Energy. 125 (2016) 453–459. https://doi.org/10.1016/j.solener.2015.12.022.
[25] W.S.M. Werner, C. Ambrosch-draxl, Optical Constants and Inelastic Electron-Scattering Data for 17 Elemental Metals, 38 (2009). https://doi.org/10.1063/1.3243762.
[26] Q. Zhang, M.S. Hadavi, K. Lee, Q. Zhang, Metal-AlN cermet solar selective coatings deposited by direct current magnetron sputtering technology, Journal of Applied Physics. 31 (1998). https://doi.org/10.1088/0022-3727/31/4/003.
[27] J. Kischkat, S. Peters, B. Gruska, M. Semtsiv, M. Chashnikova, M. Klinkmüller, O. Fedosenko, S. Machulik, A. Aleksandrova, G. Monastyrskyi, Y. Flores, W.T. Masselink, Mid-infrared optical properties of thin films of aluminum oxide, titanium dioxide, silicon dioxide, aluminum nitride, and silicon nitride, Appl. Opt. 51 (2012) 6789–6798. https://doi.org/10.1364/AO.51.006789.
[28] F. Burkholder, C.F. Kutscher, Heat loss testing of Schott's 2008 PTR70 parabolic trough receiver, NREL Technical Report. (2009) 1–58.
[29] A. Grosjean, A. Soum-Glaude, P. Neveu, L. Thomas, Comprehensive simulation and optimization of porous SiO2 antireflective coating to improve glass solar transmittance for solar energy applications, Solar Energy Materials and Solar Cells. 182 (2018) 166–177. https://doi.org/10.1016/J.SOLMAT.2018.03.040.
[30] C.C. Katsidis, D.I. Siapkas, General transfert-matrix method for optical multilayer systems with coherent, partially coherent, and incoherent interference, Applied Optics. 41 (2002) 3978–3987. https://doi.org/10.1364/AO.41.003978.
[31] R. Boidin, V. Nazabal, L. Bene, N. Petr, Pulsed laser deposited alumina thin films, Ceramics International. 42 (2016) 1177–1182. https://doi.org/10.1016/j.ceramint.2015.09.048.
[32] A.D. Rakic, A.B. Djurisic, J.M. Elazar, M.L. Majewski, Optical properties of metallic films for vertical-cavity optoelectronic devices., Applied Optics. 37 (1998) 5271–5283. https://doi.org/10.1364/AO.37.005271.
[33] M.A. Ordal, R.J. Bell, R.W. Alexander, L.L. Long, M.R. Querry, Optical properties of Au, Ni, and Pb at submillimeter wavelengths, Applied Optics. 26 (1987) 744–752. https://doi.org/10.1364/AO.26.000744.
[34] A. Fernández-García, F. Sutter, M. Montecchi, F. Sallaberry, A. Heimsath, C. Heras, E. Le Baron, A. Soum-Glaude, Parameters and method to evaluate the reflectance properties of reflector materials for concentrating solar power technology, SolarPACES Official Reflectance Guideline Version 3.0, SolarPaces. (2018).
[35] Q. Zhang, Recent progress in high-temperature solar selective coatings, Solar Energy Materials and Solar Cells. 62 (2006) 63–74. https://doi.org/10.1016/S0927-0248(99)00136-1.
[36] D. Stroud, The effective medium approximations: Some recent developments, Superlattices and Microstructures. 23 (1998) 567–573. https://doi.org/10.1006/spmi.1997.0524.

[37] D.E. Aspnes, J.B. Theeten, F. Hottier, Investigation of effective-medium models of microscopic surface roughness by spectroscopic ellipsometry, American Physical Society. 20 (1979) 3292–3302. https://doi.org/10.1103/PhysRevB.20.3292.
[38] D. Ngoue, A. Grosjean, L. Di Giacomo, S. Quoizola, A. Soum-Glaude, L. Thomas, Y. Lalau, R. Reoyo-Prats, B. Claudet, O. Faugeroux, C. Leray, A. Toutant, J.-Y. Peroy, A. Ferrière, G. Olalde, Ceramics for concentrated solar power (CSP): From thermophysical properties to solar absorbers, Advanced Ceramics for Energy Conversion and Storage. (2020) 89–127. https://doi.org/10.1016/B978-0-08-102726-4.00003-X.
[39] F. Thiel, I.M. Sokolov, Effective-medium approximation for lattice random walks with long-range jumps, Physical Review E - Statistical, Nonlinear, and Soft Matter Physics. 94 (2016) 1–11. https://doi.org/10.1103/PhysRevE.94.012135.
[40] D.R. Myers, C.A. Gueymard, Description and Availability of the SMARTS Spectral Model for Photovoltaic Applications, in: Optical Science and Technology, the SPIE 49th Annual Meeting, Denver, Colorado, United States, 2004: pp. 1–12. https://doi.org/10.1117/12.555943.
[41] ASTM G173–03 Standard Tables for Reference Solar Spectral Irradiances: Direct Normal and Hemispherical on 37° Tilted Surface, ASTM Standart. (2003). https://doi.org/10.1039/C3EE43825B.
[42] M. Planck, The theory of heat radiation, Dover Publication, INC, New York, 1914.
[43] A. Soum-Glaude, A. Le Gal, M. Bichotte, C. Escape, L. Dubost, Optical characterization of TiAlNx/TiAlNy/Al2O3 tandem solar selective absorber coatings, Solar Energy Materials and Solar Cells. 170 (2017) 254–262. https://doi.org/10.1016/j.solmat.2017.06.007.
[44] Scilab, Scilab v5.5.0, (n.d.).
[45] D. Itskhokine, Q. Lancereau, M. Benmarraze, M. Bichotte, A. Dubost, A. Soum Glaude, C. Ferrière, LFR500 project: getting to high temperature while maintaining the cost-competitive advantage of Linear Fresnel Reflectors, Energy Procedia. (2015).
[46] H.C. Barshilia, S. John, V. Mahajan, Nanometric multi-scale rough, transparent and anti-reflective ZnO superhydrophobic coatings on high temperature solar absorber surfaces, Solar Energy Materials and Solar Cells. 107 (2012) 219–224. https://doi.org/10.1016/j.solmat.2012.06.031.